Monthly Notices
of the
ROYAL ASTRONOMICAL SOCIETY

Mon. Not. R. Astron. Soc. **408,** 2083–2091 (2010) doi:10.1111/j.1365-2966.2010.17284.x

One-sided outflows/jets from rotating stars with complex magnetic fields

R. V. E. Lovelace,[1⋆] M. M. Romanova,[2⋆] G. V. Ustyugova[3⋆] and A. V. Koldoba[4⋆]

[1]*Departments of Astronomy and Applied and Engineering Physics, Cornell University, Ithaca, NY 14853, USA*
[2]*Department of Astronomy, Cornell University, Ithaca, NY 14853, USA*
[3]*Keldysh Institute of Applied Mathematics, Russian Academy of Sciences, Moscow, Russia*
[4]*Institute for Mathematical Modelling, Russian Academy of Sciences, Moscow, Russia*

Accepted 2010 July 1. Received 2010 July 1; in original form 2010 March 27

ABSTRACT

We present for the first time axisymmetric magnetohydrodynamic simulations which show the formation of intrinsically asymmetric or *one-sided* outflows or jets from disc accretion on to a rotating star with a complex magnetic field. The intrinsic magnetic field of the star is assumed to consist of a superposition of an aligned dipole and an aligned quadrupole in different proportions. The star is assumed to be rapidly rotating in the sense that the star's magnetosphere is in the propeller regime where strong outflows occur. Our simulations show that for conditions where there is a significant quadrupole component in addition to the dipole component, then a dominantly *one-sided* conical wind tends to form on the side of the equatorial plane with the larger value of the intrinsic axial magnetic field at a given distance. For cases where the quadrupole component is absent or very small, we find that dominantly one-sided outflows also form, but the direction of the flow 'flip-flops' between upward and downward on a time-scale of $\sim$30 d for a protostar. The average outflow will thus be symmetrical. In the case of a pure quadrupole field we find symmetric outflows in the upward and downward directions.

Key words: accretion, accretion discs – MHD – stars: magnetic field.

1 INTRODUCTION

There is clear evidence, mainly from *Hubble Space Telescope* (*HST*) observations, of the asymmetry between the approaching and receding jets from a number of young stars. The objects include the jets in HH 30 (Bacciotti, Eisloffel & Ray 1999), RW Aur (Woitas et al. 2002), TH 28 (Coffey et al. 2004) and LkHα 233 (Perrin & Graham 2007). Specifically, the radial speed of the approaching jet may differ by a factor of 2 from that of the receding jet. For example, for RW Aur the radial redshifted speed is $\sim$100 km s^{-1} whereas the blueshifted radial speed is $\sim$175 km s^{-1}. The mass and momentum fluxes are also significantly different for the approaching and receding jets in a number of cases. Of course, it is possible that the observed asymmetry of the jets could be due to say differences in the gas densities on the two sides of the source. Here, we investigate the case of intrinsic asymmetry where the asymmetry of outflows is connected with asymmetry of the star's magnetic field.

There is substantial observational evidence that young stars often have *complex* magnetic fields consisting of dipole, quadrupole and higher order poles possibly misaligned with respect to each other and the rotation axis (Jardine, Collier Cameron & Donati 2002; Donati et al. 2007, 2008). Analysis of matter flow around stars with realistic fields has shown that a fraction of the star's magnetic field lines are open and may carry outflows (e.g. Gregory et al. 2006).

A number of global 3D magnetohydrodynamics (MHD) simulations have been done of disc accretion on to rotating stars with complex magnetic fields. The star's intrinsic field may be a superposition of aligned or misaligned dipole and quadrupole fields (Long, Romanova & Lovelace 2007, 2008), or a superposition of dipole and octupole field components (Long, Romanova & Lamb 2010; Romanova et al. 2010). These simulations were focused on accretion processes. To study the outflows from these systems requires a much lower coronal density than assumed in these works. Intermittent outflows from the disc-magnetosphere boundary have been found in axisymmetric simulations in cases where the star has a dipole magnetic field and where symmetry about the equatorial plane was assumed (e.g. Goodson, Winglee & Böhm 1997; Goodson, Böhm & Winglee 1999).

In long-time axisymmetric (2.5D) simulations, long-lasting outflows were obtained first in the propeller regime where the star spins rapidly (Romanova et al. 2005; Ustyugova et al. 2006) and subsequently in the general case by Romanova et al. (2009, hereafter R09). In the propeller regime the outer part of the star's magnetosphere – the magnetopause – rotates more rapidly than the Keplerian rate of the accretion disc (Lovelace, Romanova & Bisnovatyi-Kogan

⋆E-mail: rvl1@cornell.edu (RVEL); romanova@astro.cornell.edu (MMR); ustyugg@rambler.ru (GVU); koldoba@rambler.ru (AVK)

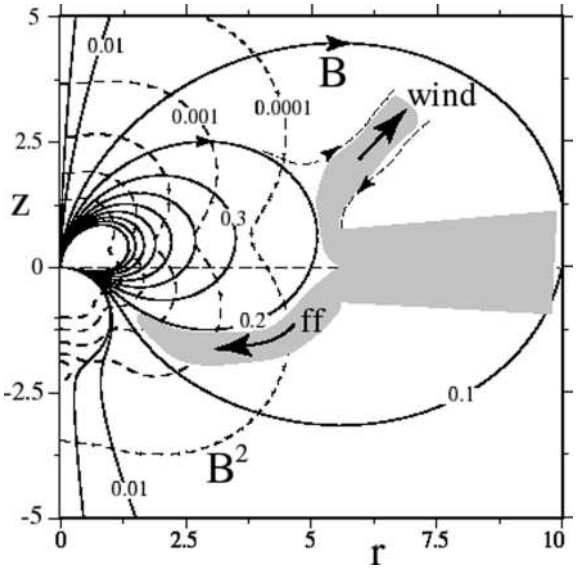

Figure 1. The magnetic field lines $\Psi(r, z) =$ constant and constant magnetic pressure lines for the case of an aligned dipole and quadrupole field where the flux function is $\Psi = \mu_{\rm d} r^2/R^3 + (3/4)\mu_{\rm q} z r^2/R^5$, where $R^2 = r^2 + z^2$ and $\mu_{\rm d}$ is the dipole moment and $\mu_{\rm q}$ is the quadrupole moment. Roughly, $\mu_{\rm q}/\mu_{\rm d}$ is the distance at which dipole and quadrupole fields are equal. The funnel flow (ff) and the wind in this figure are suggested. The dashed lines are constant values of $\boldsymbol{B}^2$.

1999). Simulations show that most of the matter outflow goes into conical-shape winds from the inner part of the disc. This wind resembles the X-wind model (Shu et al. 1994), but there are a number of important differences discussed in R09.

This paper presents for the first time MHD simulations showing the asymmetry of the jets formed by a rotating star with a *complex magnetic field*. We consider a superposition of a dipole and a quadrupole field components both aligned with the rotation axis of the star and of the disc. For such a configuration the magnetic field is *not* symmetric about the equatorial plane. This can give rise to one-sided or asymmetric magnetically driven outflows (Wang, Sulkanen & Lovelace 1992). Fig. 1 shows the nature of a combined vacuum dipole plus quadrupole field components. In this case we have sketched an extreme possibility where there is a conical wind from the top side of the disc but no outflow from the bottom side, only a funnel flow marked ff.

In this paper we present results of systematic MHD simulations of the formation of conical winds for the axisymmetric dipole/quadrupole field combinations following the approach of R09 where conical winds are found to form at the disc-magnetosphere boundary. The new aspect of this paper is that the outflows are *not* required to be symmetrical about the equatorial plane.

Section 2 of the paper describes the different aspects of the simulation model. Section 3 discusses the results of the simulations. We will quantify the asymmetry of the velocities of the top/bottom jets as well as the asymmetry of the mass and momentum fluxes for different quadrupole/dipole field strengths, different disc accretion rates and different stellar rotation rates. Section 4 gives the conclusions of this paper.

2 SIMULATION MODEL

We investigate the formation of one-sided or asymmetric jets using a set of axisymmetric numerical simulations. The arrangement of the problem is similar to that described by Ustyugova et al. (2006, hereafter U06). However, in contrast with U06, the simulations were performed in the *entire* simulation region *without* assuming symmetry about the equatorial plane. Below we describe the main aspects of the simulation model and point out the new aspects of the present model.

2.1 Basic equations

Outside of the disc the flow is described by the equations of ideal MHD. Inside the disc the flow is described by the equations of viscous, resistive MHD. In an inertial reference frame the equations are

$$\frac{\partial \rho}{\partial t} + \nabla \cdot (\rho \boldsymbol{v}) = 0, \tag{1}$$

$$\frac{\partial (\rho \boldsymbol{v})}{\partial t} + \nabla \cdot \mathcal{T} = \rho \boldsymbol{g}, \tag{2}$$

$$\frac{\partial \boldsymbol{B}}{\partial t} - \nabla \times (\boldsymbol{v} \times \boldsymbol{B}) + \nabla \times (\eta_{\rm t} \nabla \times \boldsymbol{B}) = 0, \tag{3}$$

$$\frac{\partial (\rho S)}{\partial t} + \nabla \cdot (\rho S \boldsymbol{v}) = Q. \tag{4}$$

Here, ρ is the density and S is the specific entropy; $\boldsymbol{v}$ is the flow velocity; $\boldsymbol{B}$ is the magnetic field; $\mathcal{T}$ is the momentum flux density tensor; Q is the rate of change of entropy per unit volume and $\boldsymbol{g} = -(GM/r^2)\hat{\boldsymbol{r}}$ is the gravitational acceleration due to the star, which has mass M. The total mass of the disc is assumed negligible compared to M. The plasma is considered to be an ideal gas with adiabatic index $\gamma = 5/3$ and $S = \ln(p/\rho^\gamma)$. We use spherical coordinates (r, θ, ϕ) with θ measured from the symmetry axis. The condition for axisymmetry is $\partial/\partial\phi = 0$. The equations in spherical coordinates are given in U06.

The stress tensor $\mathcal{T}$ and the treatment of viscosity and diffusivity are described in the appendix of R09. Briefly, both the viscosity and the magnetic diffusivity of the disc plasma are considered to be due to turbulent fluctuations of the velocity and the magnetic field. We adopt the standard hypothesis where the microscopic transport coefficients are replaced by turbulent coefficients. We use the α-model of Shakura & Sunyaev (1973) where the coefficient of the turbulent kinematic viscosity $\nu_{\rm t} = \alpha_v c_{\rm s}^2/\Omega_{\rm K}$, where $c_{\rm s}$ is the isothermal sound speed and $\Omega_{\rm K}(r)$ is the Keplerian angular velocity. Similarly, the coefficient of the turbulent magnetic diffusivity $\eta_{\rm t} = \alpha_d c_{\rm s}^2/\Omega_{\rm K}$. Here, α_v and α_d are dimensionless coefficients which are treated as parameters of the model.

2.2 Magnetic field of star

We consider the superposition of aligned dipole and quadrupole field components:

$$\boldsymbol{B} = \boldsymbol{B}_{\rm d} + \boldsymbol{B}_{\rm q}, \tag{5}$$

where

$$\boldsymbol{B}_{\rm d} = \frac{3\mu_{\rm d}(\hat{\boldsymbol{\mu}}_{\rm d} \cdot \hat{\boldsymbol{r}})\hat{\boldsymbol{r}}}{|\boldsymbol{r}|^3} - \frac{\mu_{\rm d}\hat{\boldsymbol{\mu}}_{\rm d}}{|\boldsymbol{r}|^3},$$

$$\boldsymbol{B}_{\rm q} = \frac{3\mu_{\rm q}(5(\hat{\boldsymbol{\mu}}_{\rm q} \cdot \hat{\boldsymbol{r}})^2 - 1)\hat{\boldsymbol{r}}}{4|\boldsymbol{r}|^4} - \frac{3\mu_{\rm q}(\hat{\boldsymbol{\mu}}_{\rm q} \cdot \hat{\boldsymbol{r}})\hat{\boldsymbol{\mu}}_{\rm q}}{2|\boldsymbol{r}|^4}. \tag{6}$$

Here, $\boldsymbol{B}_{\rm d}$ and $\boldsymbol{B}_{\rm q}$ are the magnetic fields of the dipole and quadrupole components with $\mu_{\rm d}$ and $\mu_{\rm q}$ the magnetic moments. Also, $\hat{\boldsymbol{r}}$, $\hat{\boldsymbol{\mu}}_{\rm d}$ and $\hat{\boldsymbol{\mu}}_{\rm q}$ are unit vectors for the position and the direction of

the dipole and quadrupole moments, respectively. For the considered conditions $\hat{\boldsymbol{\mu}}_{\rm d}$ and $\hat{\boldsymbol{\mu}}_{\rm q}$ are in the z-direction. The combined dipole/quadrupole field can be expressed in terms of the flux function $\Psi = \mu_{\rm d} r^2/R^3 + (3/4)\mu_{\rm q} z r^2/R^5$, where the field lines correspond to $\Psi(r, z) =$ constant. Here, we briefly use cylindrical coordinates (r, ϕ, z), with $R^2 = r^2 + z^2$, $B_r = -(1/r)\partial\Psi/\partial z$ and $B_z = (1/r)\partial\Psi/\partial r$.

2.3 Reference units

The MHD equations are solved in dimensionless form so that the results can be readily applied to different accreting stars. We take the reference mass M_0 to be the mass M of the star. The reference radius is taken to be *twice* the radius of the star, $R_0 = 2 \times R_*$. The reference velocity is $v_0 = (GM/R_0)^{1/2}$ and the reference angular velocity $\Omega_0 = 1/t_0$. We measure time in units of $P_0 = 2\pi t_0$, which is the Keplerian rotation period of the disc at $r = R_0$. In the plots we use the dimensionless time $T = t/P_0$.

The dimensionless dipole and quadrupole magnetic moments are

$$\tilde{\mu}_{\rm d} \equiv \frac{\mu_{\rm d}}{B_0 R_0^3}, \quad \tilde{\mu}_{\rm q} \equiv \frac{\mu_{\rm q}}{B_0 R_0^4}, \tag{7}$$

where B_0 is the reference magnetic field. Taking into account that $\mu_{\rm d} = B_{\rm d\star} R_\star^3 = B_0 R_0^3 \tilde{\mu}_{\rm d}$, we find $B_0 = B_{\rm d\star}(R_\star/R_0)^3/\tilde{\mu}_{\rm d}$, where $B_{\rm d\star}$ is the equatorial dipole magnetic field strength on the surface of the star.

The reference density is taken to be $\rho_0 = B_0^2/v_0^2$. The reference pressure is $p_0 = B_0^2$. The reference temperature is $T_0 = p_0/\mathcal{R}\rho_0 = v_0^2/\mathcal{R}$, where $\mathcal{R}$ is the gas constant. The reference accretion rate is $\dot{M}_0 = \rho_0 v_0 R_0^2$. The reference energy flux is $\dot{E}_0 = \dot{M}_0 v_0^2$. The reference angular momentum flux is $\dot{L}_0 = \dot{M}_0 v_0 R_0$.

The reference units are defined in such a way that the dimensionless MHD equations have the same form as the dimensional ones, equations (1)–(4). For the non-dimensionalization we put $GM = 1$ and $\mathcal{R} = 1$. We solve MHD equations (1)–(4) using normalized variables: $\tilde{\rho} = \rho/\rho_0$, $\tilde{v} = v/v_0$, $\tilde{B}_{\rm d} = B_{\rm d}/B_0$, $\tilde{B}_{\rm q} = B_{\rm q}/B_0$, etc. Most of the plots show the normalized variables (with the tildes implicit). The conversion factors for recovering the physical values for protostars, brown dwarfs, white dwarfs and neutron stars are given in table 1 of Romanova et al. (2009).

2.4 Initial and boundary conditions

The initial and boundary conditions are the same as those used in U06. Here, we summarize these conditions.

Initial conditions. A star of mass M is located at the origin of the coordinate system. A cold disc and hot corona are initialized in the simulation region. The disc is of low temperature $T_{\rm d}$ and high density $\rho_{\rm d}$. The corona is of high temperature $T_{\rm c} \gg T_{\rm d}$ and low density $\rho_{\rm c} \ll \rho_{\rm d}$ and it fills all other space but the disc. The disc extends inward to a radius $r_{\rm d} = 5$ and rotates with Keplerian angular velocity $\omega \approx \Omega_{\rm K}$. In reality, it is slightly sub-Keplerian, $\Omega(\theta = \pi/2) = \kappa\Omega_{\rm K}(\kappa = 1\text{–}0.003)$, due to which the density and pressure decrease towards the periphery. Initially, at any cylindrical radius r from the rotation axis, we rotate the corona and the disc at the same angular rate. This avoids a jump discontinuity of the angular velocity of the plasma at the boundary between the disc and the corona. Inside the cylinder $r \le r_{\rm d}$, the matter of the corona rotates rigidly with angular velocity $\Omega(r_{\rm d}) = \kappa(GM/r_{\rm d}^3)^{1/2}$. For a gradual start-up we change the angular velocity of the star from its initial value $\Omega(r_{\rm d}) = 5^{-3/2} \approx 0.09(r_{\rm d} = 5)$ to a final value of $\Omega_* = 1$ over the course of three Keplerian rotation periods at $r = 1$.

In most simulation runs we fix the dipole moment of the star as $\tilde{\mu}_{\rm d} = 10$ and vary the quadrupole moment as $\tilde{\mu}_{\rm q} = 0$, 1, 10, 20, 30, 40, 60. We also have test cases of $\tilde{\mu}_{\rm d} = 0$ and $\tilde{\mu}_{\rm q} = 20$, 60. The angular velocity of the star in the propeller regime is $\Omega_* = 1$ and this corresponds to the corotation radius of $r_{\rm cor} = 1$. The initial density in the disc at the fiducial point (at the inner edge) is $\rho_{\rm d} = 1$, initial density in the corona $\rho_{\rm c} = 0.0003$. The gas in the corona is hot with initial temperature $T_{\rm c} = 1$ and the disc is cold with temperature $T_{\rm d} = (\rho_{\rm c}/\rho_{\rm d})T_{\rm c} = 3 \times 10^{-4}$. There is initial pressure equilibrium at the disc–corona boundary.

The coefficients of viscosity and diffusivity are taken to be $\alpha_v = 0.3$ and $\alpha_d = 0.1$ (as in R09).

Boundary conditions. The boundary conditions at the inner boundary $r = R_{\rm in}$ are the following. The frozen-in condition is applied to the poloidal component $\boldsymbol{B}_{\rm p}$ of the field, such that B_r is fixed while B_θ and B_ϕ obey 'free' boundary conditions, $\partial B_\theta/\partial r = 0$ and $\partial B_\phi/\partial r = 0$. The density, pressure and entropy also have free boundary conditions, $\partial(\ldots)/\partial r = 0$. The velocity components are calculated using free boundary conditions. Then, the velocity vector is adjusted to be parallel to the magnetic field vector in the coordinate system rotating with a star. Matter always flows inward at the star's surface. Outflow of a wind from the stellar surface is not considered in this paper. The boundary conditions at the external boundary $r = R_{\rm out}$ in the *coronal region* $0 < \theta < \theta_{\rm d1}$ and $\theta_{\rm d2} < \theta \le \pi$ are free for all hydrodynamic variables. Here, $\theta_{\rm d1}$ corresponds to the top surface of the disc and $\theta_{\rm d2}$ to the bottom surface. We prevent matter from flowing into the simulation region from this part of the boundary. We solve the transport equation for the flux function Ψ so that the magnetic flux flows out of the region together with matter. If the matter has a tendency to flow back in, then we fix Ψ. In the disc region, restricted by two values of θ ($\theta_{\rm d1} < \theta < \theta_{\rm d2}$), we fix the density at $\rho = \rho_{\rm d}$, and establish a slightly sub-Keplerian velocity, $\Omega_{\rm d} = \kappa\Omega(r_{\rm d})$, where $\kappa = 1\text{–}0.003$ so that matter flows into the simulation region through the boundary. The inflowing matter has a fixed magnetic flux which is very small because $R_{\rm out} \gg R_{\rm in}$.

The system of MHD equations (1–4) was integrated numerically using the Godunov-type numerical scheme (see appendix of R09). The simulations were done in the region $R_{\rm in} \le r \le R_{\rm out}$, $0 \le \theta \le \pi$. The grid is uniform in the θ-direction. The size steps in the radial direction were chosen so that the poloidal-plane cells were curvilinear rectangles with approximately equal sides. A typical region for investigation of asymmetric winds was $1 \le r \le 40$, with grid resolution $N_r \times N_\theta = 104 \times 80$ cells. The simulation domain has 13 slices in the radial direction and 10 slices in θ-direction. Each simulation run takes 4–12 d on 130 processors of the NASA high-performance facilities. Cases with stronger quadrupole component require longer simulations. The simulation time increases with increase of the quadrupole moment, and hence the longest simulations are those at $\tilde{\mu}_{\rm q} = 60$. Test runs were also performed at the lower grid of 80×60 and higher grid of 160×120 which show similar results (approximately the same matter flux on to the star and into the winds), though the latter grids require more computer resources. Simulations with the grid of 80×60 were used for a number of exploratory runs.

3 RESULTS

3.1 Properties of one-sided outflows

Here, we chose one case with intermediate parameters: $\mu_{\rm d} = 10$, $\mu_{\rm q} = 20$, call it 'the main case', and show it in greater detail

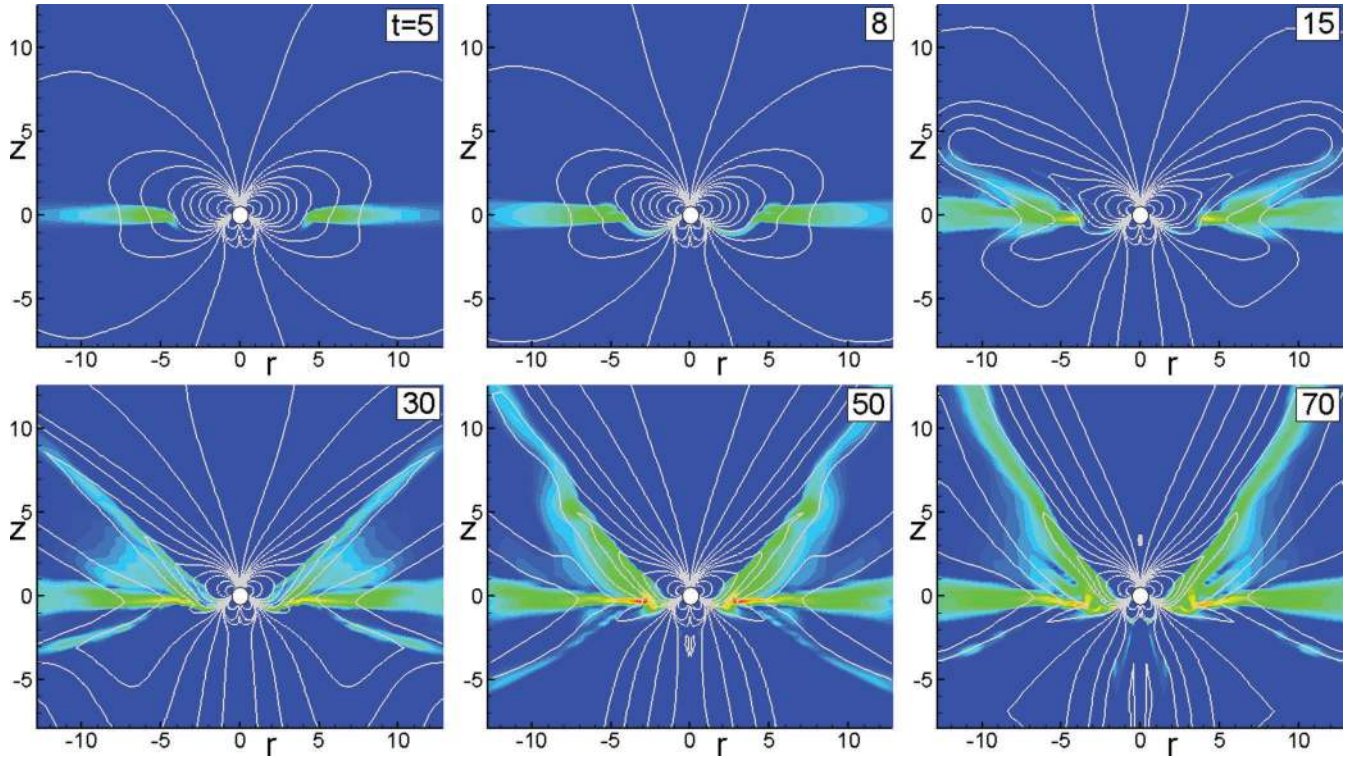

Figure 2. Development of an asymmetric jet in the main case ($\tilde{\mu}_{\rm d} = 10$, $\tilde{\mu}_{\rm q} = 20$). The colour background shows the matter flux density. The lines are the poloidal field lines. The simulations are shown at different times t, which is measured in periods of rotation of the disc at $r = 1$.

compared with other cases. Fig. 2 shows formation of asymmetric outflows. One can see that initially, at $t = 5$–8 orbits, matter starts to accrete on to the star along the shortest path, towards the quadrupolar belt, which is below the equator. Later, at $t \approx 15$ orbits, the disc matter diffused through the external closed field lines of the top and bottom parts of the magnetosphere, these lines inflated, and the conical-type wind starts to blow along these field lines. Most of the matter outflows from the top side of the disc, where the magnetic field is stronger. Outflows are episodic but quasi-steady on average. The episodic nature is connected with accumulation of matter near the closed magnetosphere, diffusion through closed field lines, inflation of these lines, outburst to the wind and enhanced accretion on to the star (see also Goodson & Winglee 1999; U06; R09). Fig. 3 shows larger view of typical, well-developed outflows at $t = 50$ orbits. One can see that outflows are more powerful on the top side of the disc and much less powerful on the bottom side.

The mechanism of the outflow formation is similar to that in cases of conical winds (R09): the magnetic flux of the star is pushed towards the star and compressed by the disc so that the poloidal field lines are always inclined relative to the disc. In addition, the rotating magnetosphere acts to make the field lines to rotate with a super-Keplerian velocity. These field lines thread the corona which rotates more slowly. Consequently there is a strong winding up of the field lines just above the disc. Hence a strong magnetic force appears, $F_{\rm m} = -\nabla(r^2 B_\phi^2)$, which drives matter down the gradient of the magnetic pressure (Lovelace, Berk & Contopoulos 1991). Fig. 4 shows the poloidal current through a disc of radius r, $I_{\rm p} \propto r B_\phi$. One can see that matter flows to the conical-type winds and is driven by the magnetic force. Ohmic heating is included in our code, but it does not have a significant role in the jet launching. Fig. 5 shows the initial distribution of the specific entropy and that at $t = 50$ orbits. One can see that the low-entropy (cold) matter from the disc flows to the winds above and below the disc. On the top side of the disc this cold matter pushes the hot coronal gas towards the axis. On the bottom side of the disc, the hot coronal gas is pushed away and is gradually replaced by cold gas from the disc.

3.2 One-sided outflows for different quadrupole moments

In this section we compare asymmetric outflows obtained in a set of simulations where we fixed the dipole component of the field at $\tilde{\mu}_{\rm d} = 10$ and varied the quadrupolar component from very small up to very large values: $\tilde{\mu}_{\rm q} = 1$, 10, 20, 30, 40, 60. Fig. 6 shows an initial magnetic field distribution in a number of cases. Fig. 6 shows that at $\tilde{\mu}_{\rm q} = 1$ the quadrupole component is very small and the magnetic field is almost pure dipole field, while for $\tilde{\mu}_{\rm q} = 40$, 60 the quadrupole field dominates. Fig. 7 shows asymmetric outflows at $t = 50$ orbits. One can see that in all cases most of the matter outflows above the disc, to the side where the intrinsic magnetic field is stronger. At the same time there is a much weaker matter flux from the other side of the disc.

We calculated the matter fluxes to outflows through a spherical surface of radius $r = 10$:

$$\dot{M} = \int {\rm d}\boldsymbol{S} \cdot \rho \boldsymbol{v}_{\rm p}, \tag{8}$$

where ${\rm d}\boldsymbol{S}$ is the surface area element directed outward. Fig. 8 shows matter fluxes above and below the disc for cases with different $\tilde{\mu}_{\rm q}$. One can see that the main, upward outflows, have similar matter fluxes for $\tilde{\mu}_{\rm q} = 40$ and $\tilde{\mu}_{\rm q} = 60$, while at lower quadrupole moment $\tilde{\mu}_{\rm q} = 20$ matter flux is higher. The matter fluxes of the downward

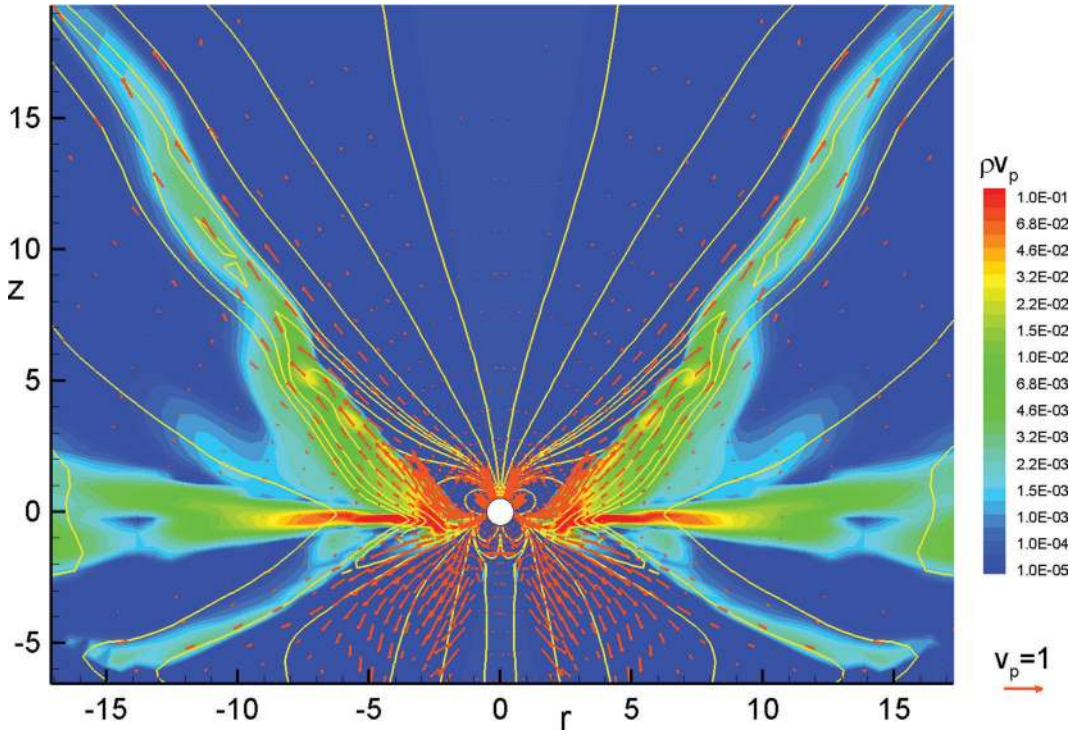

Figure 3. Enlarged snapshot of the outflow in the main case ($\tilde{\mu}_{\rm d} = 10$, $\tilde{\mu}_{\rm q} = 20$) at $t = 50$ orbits. The colour background shows the matter flux density and the lines are the poloidal field lines. The vectors show the poloidal velocity.

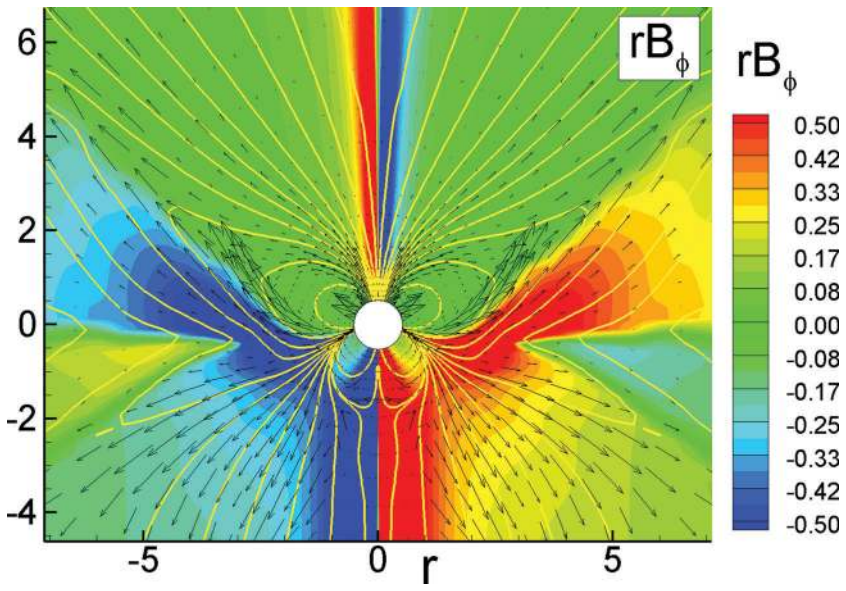

Figure 4. The colour background shows $r B_\phi(r, z)$ at $t = 50$ orbits, which is proportional to the poloidal current flow through a circular disc of radius r at a distance z. The lines are poloidal field lines and the arrows show the poloidal velocity. For this case $\tilde{\mu}_{\rm d} = 10$ and $\tilde{\mu}_{\rm q} = 20$.

outflows (bottom set of curves in Fig. 8) are similar for all three cases and are four to eight times smaller than the main, upward outflows.

3.3 Comparison of magnetic moments

Below, we discuss the relative strengths of the dipole and quadrupole components of the field. For this it is useful to consider the dipole and quadrupole field components in the equatorial plane, $B_{\rm dz} = -\mu_{\rm d}/r^3$ and $B_{\rm qr} = -3\mu_{\rm q}/4r^4$. The radius at which $|B_{\rm dz}| = |B_{\rm qr}|$ is

$$r_{\rm eq} = \frac{3}{4}\frac{\mu_{\rm q}}{\mu_{\rm d}} \quad \text{or} \quad r_{\rm eq} = \frac{3}{4}\frac{\tilde{\mu}_{\rm q}}{\tilde{\mu}_{\rm d}} R_0 = \frac{3}{2}\frac{\tilde{\mu}_{\rm q}}{\tilde{\mu}_{\rm d}} R_\star, \tag{9}$$

where we took into account that $R_0 = 2R_\star$. We can estimate this radius for all cases above where $\tilde{\mu}_{\rm d} = 10$ and quadrupolar moments, $\tilde{\mu}_{\rm q} = 1, 10, 20, 30, 40, 60$. We obtain $\tilde{r}_{\rm eq} = (0.15, 1.5, 3.0, 4.5, 6.0, 9.0) R_\star$. Hence, the quadrupole component is dynamically important in all cases, except $\tilde{\mu}_{\rm q} = 1$, and is

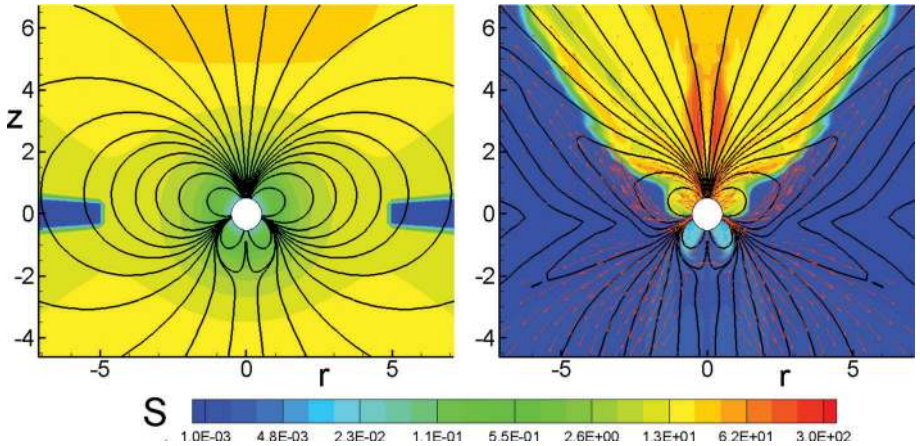

Figure 5. The colour background shows the distribution of the specific entropy S. The left-hand panel shows initial distribution and the right-hand panel shows the distribution at $t = 50$ orbits. The lines are poloidal field lines. For this case $\tilde{\mu}_{\rm d} = 10$ and $\tilde{\mu}_{\rm q} = 20$.

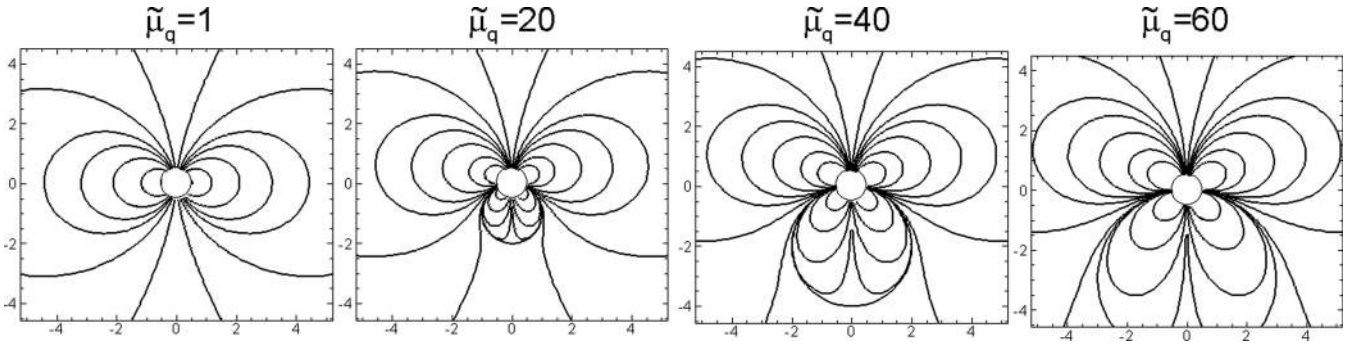

Figure 6. The figure shows the initial poloidal field lines for a fixed dipole moment $\mu_{\rm d} = 10$ and different quadrupolar moments, $\mu_{\rm q} = 0$, 20, 30, 40. The field lines have the same value of the flux function in all plots.

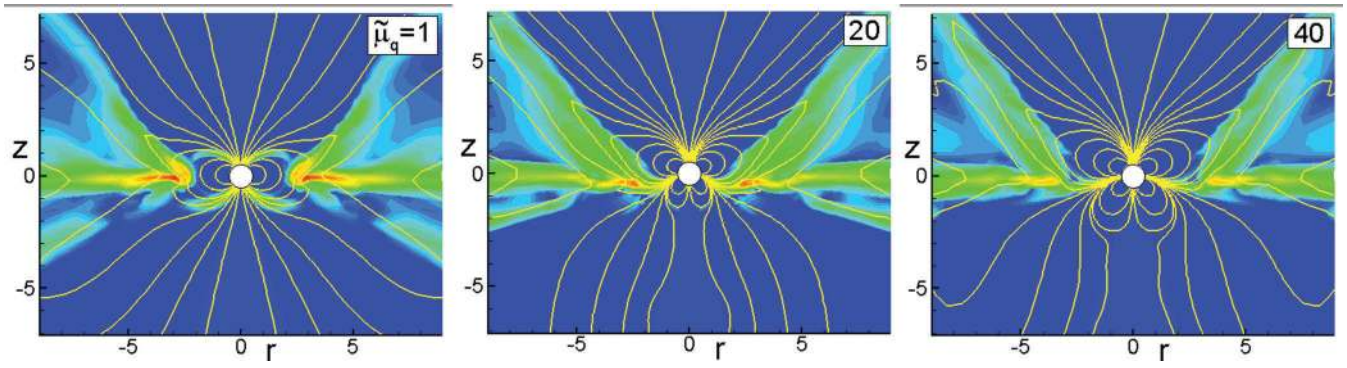

Figure 7. Outflows for different quadrupole strengths $\mu_{\rm q}$ but the same dipole component $\mu_{\rm d} = 10$ at $t = 50$ orbits. The colour background shows the matter flux density distribution. The lines are poloidal magnetic field lines.

expected to influence, e.g. the matter flow around the star at $r > r_{\rm eq}$ (Long et al. 2010; Romanova et al. 2009). However, we see that the quadrupole component determines the 'one-sidedness' and the direction of the matter outflow even for very small values, such as of $\tilde{\mu}_{\rm q} = 1$.

3.4 'Flip-flop' of outflows for a pure dipole field

For a pure dipole field, we observe one-sided outflows which reverse directions episodically. In past simulations the MHD equations were solved only in the upper half-space and it was *assumed* that the full flow was given by reflecting the top flow about the equatorial plane (U06; R09). However, in this paper we calculate the disc and outflows in the entire space above and below the equatorial plane. We discover that during a brief initial time, $t \lesssim 15$, the outflows are symmetric about the equatorial plane (see Fig. 9, top left-hand panel). However, later the outflows become strongly asymmetric with the direction of the main flow downward. This happens because the accreting funnel stream pushes part of the magnetic field downward so that the accretion path becomes shorter and more energetically favourable in the top hemisphere (see top middle plot of Fig. 9). However, after an episode of a strong outflow to winds (which is accompanied by an episode of enhanced accretion towards the star), the magnetosphere expands and there is a 'loss of memory' of the

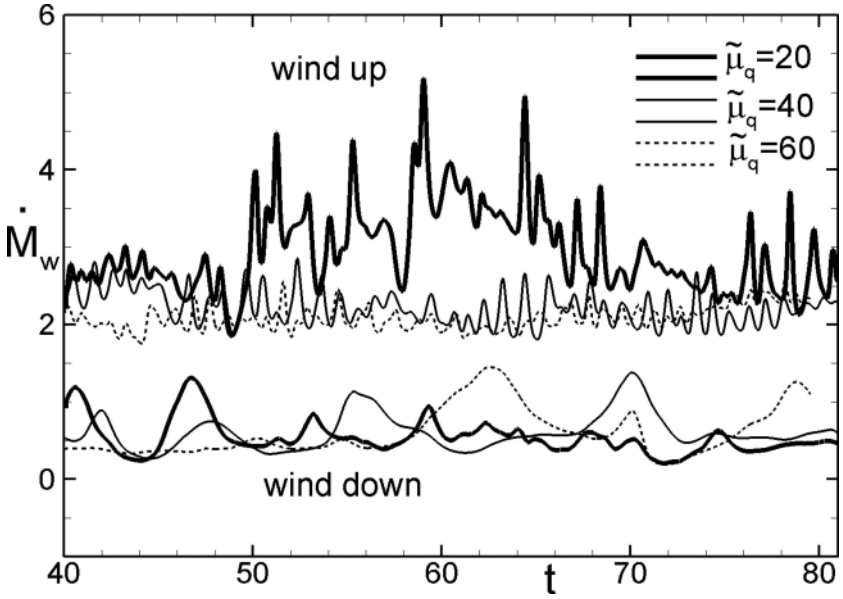

Figure 8. Matter fluxes through a hemispherical surface of radius $r = 10$ above the equatorial plane (top set of curves) and below the equatorial plane (bottom set of curves) for cases with $\tilde{\mu}_d = 10$ and different quadrupole moments of $\tilde{\mu}_q = 20, 40, 60$.

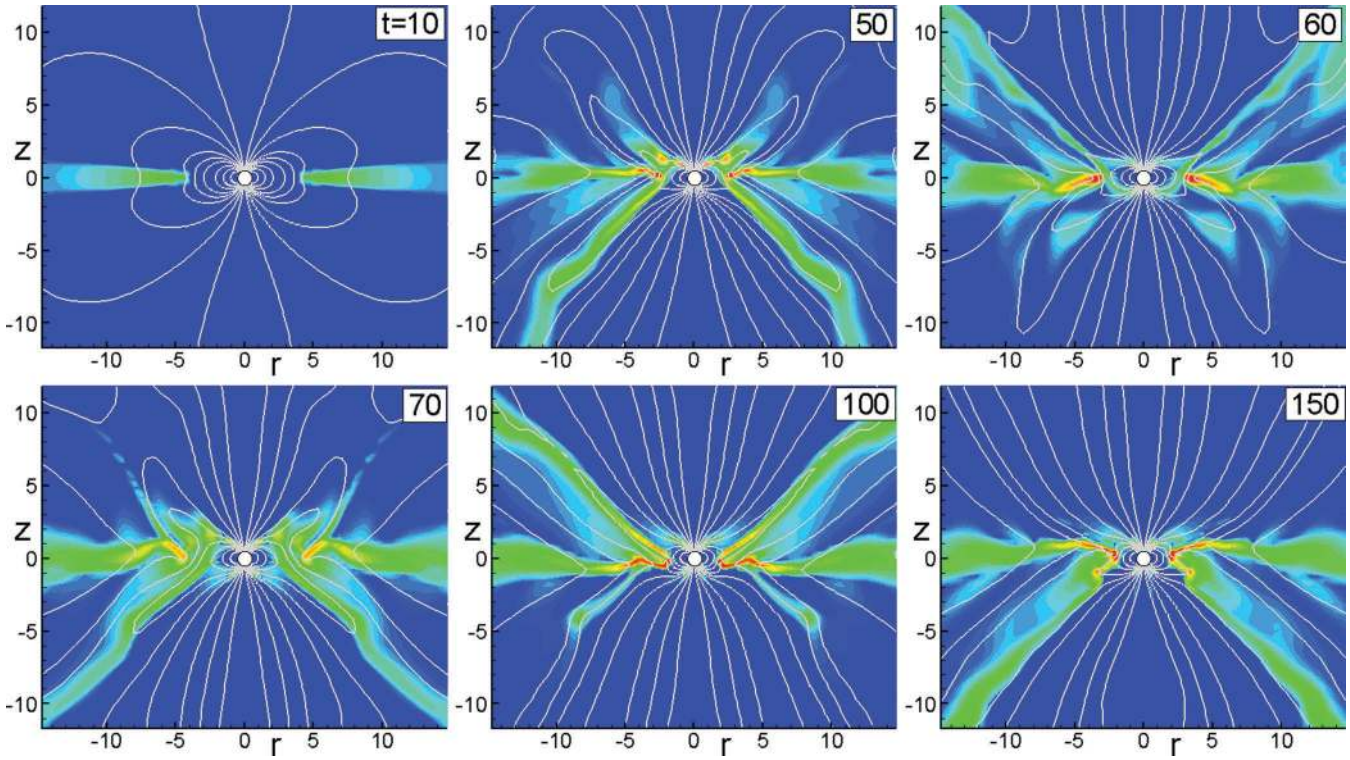

Figure 9. 'Flip-flop'of outflows in case of a pure dipole field ($\tilde{\mu}_q = 0$, $\tilde{\mu}_d = 10$. Colour background shows the matter flux distribution, and lines are the magnetic field lines.

direction of the asymmetry. As a result, the funnel stream may take a path below the disc, and consequently the dominant outflow is in the top hemisphere (see right-hand top panel of Fig. 9). We observed this 'switching' a number of times, all after strong outbursts.

The matter fluxes calculated through hemispherical surfaces with radius $r = 10$ above and below the disc also show this 'flip-flop' behaviour (see Fig. 10). The time-scale between the reversal of the direction of outflows is about 30 rotation periods. For classical T Tauri stars, this is about 30 d. We suggest that this time-scale is of the order of the magnetic field diffusion time $\tau_B = r_m^2/\eta_t$ at the magnetospheric radius r_m (see also Goodson & Winglee 1999).

3.5 Symmetric outflows for a pure quadrupole field

We performed simulations of outflows in the case of a pure quadrupole field with $\tilde{\mu}_q = 40, 60 (\tilde{\mu}_d = 0)$. Fig. 11 shows

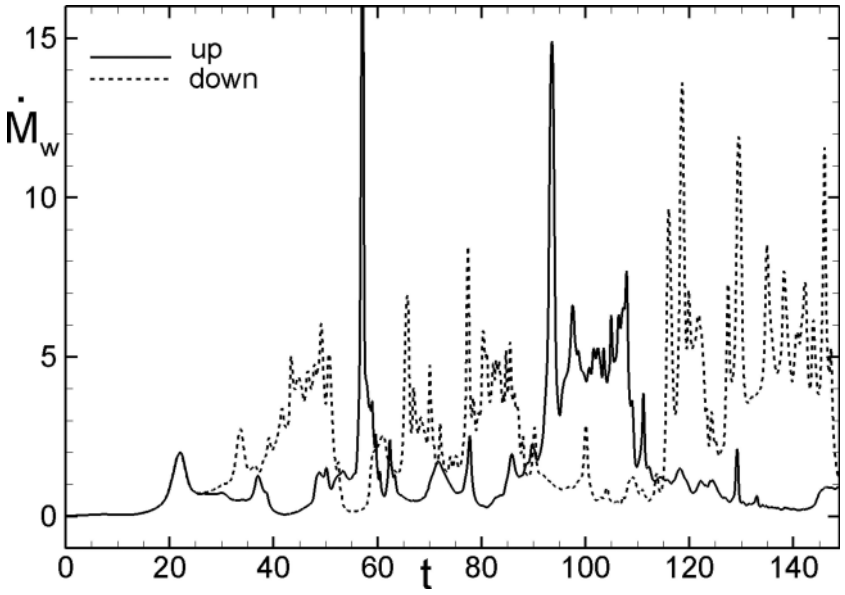

Figure 10. Matter fluxes calculated through the spherical radius $r = 10$ above the equatorial plane (solid lines) and below the equatorial plane (dashed lines) for the case of pure dipole field, $\tilde{\mu}_{\rm d} = 10$ and $\tilde{\mu}_{\rm q} = 0$.

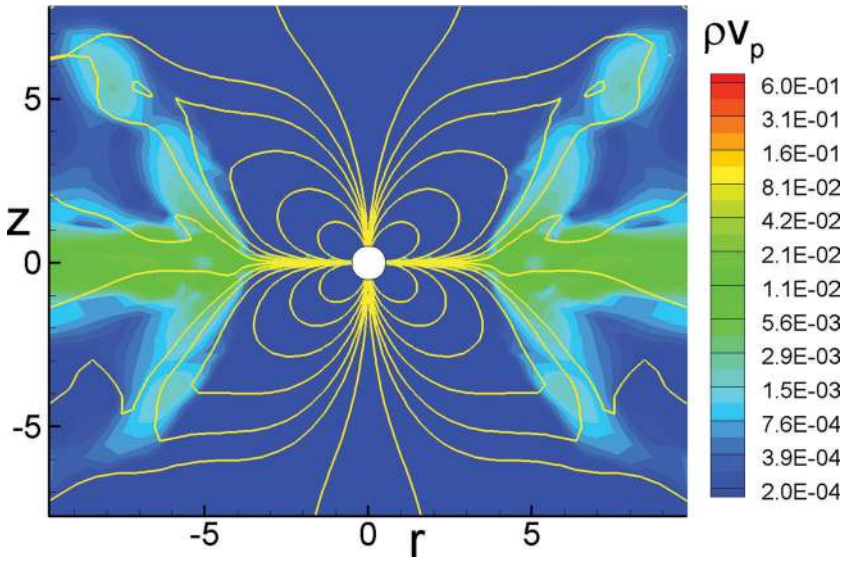

Figure 11. Matter flux density for the case of a pure quadrupole field with $\tilde{\mu}_{\rm q} = 60$. The upward and downward outflows are approximately equal.

simulation results at $t = 50$ orbits for a case with $\tilde{\mu}_{\rm q} = 60$. In this case the outflows are almost symmetric about the equatorial plane. However, in a test case with very small dipole magnetic field, $\tilde{\mu}_{\rm d} = 1$, we found that the flow is one-sided and matter flows towards the direction of the larger intrinsic magnetic field.

4 CONCLUSIONS

We performed axisymmetric MHD simulations of disc accretion on to rotating magnetized stars. The star's intrinsic magnetic field was assumed to consist of a superposition of aligned dipole and quadrupole components. This field configuration is *not* in general symmetric about the equatorial plane. Thus the calculations must be done in both the upper and lower half-spaces. The star was assumed to be rapidly rotating with the magnetosphere in the propeller regime (U06). The ratio of the turbulent viscosity to the turbulent magnetic diffusivity in the disc was considered to be larger than unity so that the magnetic field threading the disc is advected inward (U06; R09). The main findings are the following.

(1) For cases with both dipole and quadrupole components, a one-sided conical wind forms and persistently blows in one direction. The favoured direction is that of larger magnitude intrinsic axial magnetic field. Much weaker outflows form on the opposite side of the disc. The physical reason for the one-sided outflow is that a funnel flow naturally develops in the hemisphere with the shorter field aligned path to the star's surface as indicated in Fig. 1. Thus the matter which for symmetrical conditions (about the equatorial plane) would go into an outflow instead falls to the surface of the star.

(2) For the case of a pure dipole field, the outflows are also one-sided, but the outflow direction alternates or 'flip-flops' on a time-scale of about 30 d for a T Tauri star.

(3) For the case of a pure quadrupole field, symmetric outflows form. However, the presence of even a very small dipole component leads to one-sided outflows.

Note that outflows from a T Tauri star may change direction due to variations of the star's magnetic field on a time-scale of months (Smirnov et al. 2004). If the complex field of a star is determined by dynamo processes inside the star, then one or another hemisphere may have the stronger axial magnetic field which determines the direction of the outflow.

An intrinsic asymmetry of the outflows or jets will give a net force on the protostar by analogy with the previously analysed case of asymmetric jets from magnetized black hole discs (Wang et al. 1992; Tsygan 2007; Korneich & Lovelace 2008). If the outflow is one-sided for a long time T with asymptotic velocity $V_{\rm j}$ and mass flux $\dot{M}_{\rm j}$, then the velocity imparted to the star is $\Delta v_* = \dot{M}_{\rm j} V_{\rm j} T / M_*$. For example, for a T Tauri star with $\dot{M}_{\rm j} = 10^{-8}\,{\rm M}_\odot\,{\rm yr}^{-1}$, $V_{\rm j} = 3 \times 10^7\,{\rm cm\,s}^{-1}$, $T = 10^5$ yr and $M_* = {\rm M}_\odot$, we find $\Delta v_* = 3 \times 10^4\,{\rm cm\,s}^{-1}$ which is probably undetectable. For the case of an almost pure dipole field the frequent 'flip-flops' of the outflow direction will cause the star to random walk but the net displacement and velocity are very small.

In addition to the intrinsic stellar magnetic field considered here, the accretion disc can advect inward external (e.g. interstellar) magnetic flux because of the disc's highly conducting (non-turbulent) surface layers (Bisnovatyi-Kogan & Lovelace 2007; Rothstein & Lovelace 2008; Lovelace, Rothstein & Bisnovatyi-Kogan 2009). The combination of the advected field and the intrinsic field of the star can give rise to a complex field structure near the star's magnetopause which produces asymmetric or one-sided outflows. The field of the star may be dynamo generated with a complex time-dependent structure (e.g. von Rekowski & Brandenburg 2006). In the case of disc accretion to a black hole, a large-scale asymmetric magnetic field close to the black hole can arise from advection of external flux due to the conducting surface layers of the disc or it may arise from dynamo processes in the disc which generate both dipole and quadrupole field components (e.g. Pariev & Colgate 2007; Pariev, Colgate & Finn 2007). Dynamo processes may also be important in the discs of accreting stars.

ACKNOWLEDGMENTS

We thank F. Bacciotti for a valuable discussion. This work was supported in part by NASA grants NNX08AH25G and NNX10AF63G and by NSF grant AST-0807129. MMR thanks NASA for use of the NASA High Performance Computing Facilities. AVK and GVU were supported in part by grant RFBR 09-02-00502a, Programme 4 of RAS.

REFERENCES

Bacciotti F., Eisloffel J., Ray T. P., 1999, A&A, 350, 917
Bisnovatyi-Kogan G. S., Lovelace R. V. E., 2007, ApJ, 667, L167
Coffey D., Bacciotti F., Woitas J., Ray T. P., Eislöffel J., 2004, ApJ, 604, 758
Donati J.-F. et al., 2007, MNRAS, 380, 1297
Donati J.-F. et al., 2008, MNRAS, 386, 1234
Goodson A. P., Winglee R. M., 1999, ApJ, 524, 159
Goodson A. P., Winglee R. M., Böhm K.-H., 1997, ApJ, 489, 199
Goodson A. P., Böhm K.-H., Winglee R. M., 1999, ApJ, 524, 142
Gregory S. G., Jardine M., Simpson I., Donati J.-F., 2006, MNRAS, 371, 999
Jardine M., Collier Cameron A., Donati J.-F., 2002, MNRAS, 333, 339
Korneich D. A., Lovelace R. V. E., 2008, ApJ, 681, 104
Long M., Romanova M. M., Lovelace R. V. E., 2007, MNRAS, 374, 436
Long M., Romanova M. M., Lovelace R. V. E., 2008, MNRAS, 386, 1274
Long M., Romanova M. M., Lamb F. K., 2010, MNRAS, preprint (arXiv:0911.5455)
Lovelace R. V. E., Berk H. L., Contopoulos J., 1991, ApJ, 379, 696
Lovelace R. V. E., Romanova M. M., Bisnovatyi-Kogan G. S., 1999, ApJ, 514, 368
Lovelace R. V. E., Rothstein D. M., Bisnovatyi-Kogan G. S., 2009, ApJ, 701, 885
Pariev V. I., Colgate S. A., 2007, ApJ, 658, 129
Pariev V. I., Colgate S. A., Finn J. M., 2007, ApJ, 658, 129
Perrin M. D., Graham J. R., 2007, ApJ, 670, 499
Romanova M. M., Ustyugova G. V., Koldoba A. V., Lovelace R. V. E., 2005, ApJ, 635, L165
Romanova M. M., Ustyugova G. V., Koldoba A. V., Lovelace R. V. E., 2009, MNRAS, 399, 1802 (R09)
Romanova M. M., Long M., Lamb F. K., Kulkarni A. K., Donati J.-F., 2010, MNRAS, preprint (arXiv:0912.1681)
Rothstein D. M., Lovelace R. V. E., 2008, ApJ, 677, 1221
Shakura N. I., Sunyaev R. A., 1973, A&A, 24, 337
Shu F., Najita J., Ostriker E., Wilkin F., Ruden S., Lizano S., 1994, ApJ, 429, 781
Smirnov D. A., Lamzin S. A., Fabrika S. N., Chuntonov G. A., 2004, Astron. Lett., 30, 456
Tsygan A. I., 2007, Astron. Rep., 51, 97
Ustyugova G. V., Koldoba A. V., Romanova M. M., Lovelace R. V. E., 2006, ApJ, 646, 304 (U06)
von Rekowski B., Brandenburg A., 2006, Astron. Nachr., 327, 53
Wang J. C. L., Sulkanen M. E., Lovelace R. V. E., 1992, ApJ, 390, 46
Woitas J., Ray T. P., Bacciotti F., Davis C. J., Eislöffel J., 2002, ApJ, 580, 336

This paper has been typeset from a TEX/LATEX file prepared by the author.